Population analysis and immunologic landscape of melanoma in people living with HIV

Lindsay N Barger[1,2,3], Derek Wang[4], Ashley Saravia[3], Valeria Mezzano[5,6], Gyles Ward[6], Cynthia Loomis[5,6], Carly Feldman[7], Madalina Tuluc[8], Rino S Seedor[7,2], Peter J Gaskill[1,2], Anna E Coghill[9], Gita Suneja[10], Iman Dehzangi[4,11,12], Jennifer L Hope[3,2], George Jour[5,13], Gabriele Romano[1,2]*

[1]Department of Pharmacology and Physiology, Drexel University College of Medicine, Philadelphia, Pennsylvania.

[2]Immune Cell Regulation & Targeting Program, Sidney Kimmel Comprehensive Cancer Center, Philadelphia, Pennsylvania.

[3]Department of Microbiology and Immunology, Drexel University College of Medicine, Philadelphia, Pennsylvania.

[4]Center for Computational and Integrative Biology (CCIB), Rutgers University, Camden, New Jersey

[5]Department of Pathology, New York University Langone Medical Center, New York, New York

[6]Experimental Pathology, Division of Advanced Research Technologies, New York University Langone Medical Center, New York, New York.

[7]Department of Medical Oncology, Thomas Jefferson University Hospital, Philadelphia, Pennsylvania.

[8]Department of Pathology and Genomic Medicine, Jefferson University Hospital, Philadelphia, Pennsylvania.

[9]Cancer Epidemiology Program, Moffitt Cancer Center, Tampa, Florida

[10]Department of Radiation Oncology, Huntsman Cancer Institute, Salt Lake City, Utah

[11]Department of Computer Science, Rutgers University, Camden, New Jersey

[12]Rutgers Cancer Institute, Rutgers University, New Brunswick, New Jersey

[13]Department of Dermatology, New York University Langone Medical Center, New York, New York

***Correspondence:** Gabriele Romano – gr476@drexel.edu

Keywords: melanoma, HIV, T cells, MDSCs, immunotherapy, chronic infection

Funding: G.R. is supported by: WW Smith Charitable Trust - Medical Research Program (#C2303); Department of Defense - Congressionally Directed Medical Research Programs, Melanoma Research Program (ME220048); American Cancer Society (DBG-23-1036360-01); Comprehensive NeuroHIV Center (CNHC) Developmental Research and Mentoring Core (NIMH - P30MH092177); Sidney Kimmel Comprehensive Cancer Center (#00023568 and #901333). L.B. is supported by the Translational Research Training Grant in NeuroHIV (NIMH, T32-MH079785). Experimental Pathology Research Laboratory [RRID: SCR_017928] is partially supported by the Cancer Center Support Grant (P30CA016087). The original Akoya/PerkinElmer Vectra® multispectral imaging system was awarded through the Shared Instrumentation Grant S10 OD021747.

Acknowledgments: We thank the AIDS and Cancer Specimen Resource (ACSR) for providing tumor samples from PLWH; ACSR is funded by the National Cancer Institute.

Abstract

People living with HIV (PLWH) diagnosed with melanoma have consistently exhibited worse clinical outcomes than HIV-negative individuals (PLw/oH) with the same cancer, even in the era of antiretroviral therapy (ART). To investigate the underlying factors contributing to these disparities, we analyzed electronic health records from 922 PLWH and 334,972 PLw/oH with melanoma. PLWH were diagnosed with melanoma at a younger age and had a higher representation of Hispanic and Black individuals. Notably, PLWH had a markedly increased risk of brain metastases. Additionally, despite similar treatment durations, PLWH experienced significant delays in initiating immune checkpoint therapy (ICI) and exhibited worse survival outcomes at both five- and ten-years post-treatment with ICI.

To explore potential biological determinants of these disparities, we conducted spatial immune transcriptomics on melanoma tumors (n=11). This analysis revealed a more immunosuppressive tumor landscape in PLWH, characterized by upregulated immune checkpoints (e.g., *PD1, LAG3, CTLA4)* and diminished antigen presentation (e.g., *HLA-DRB, B2M*), with distinct spatial distributions in the tumors versus the tumor microenvironments. Downstream validation via multiplex immunofluorescence (n=15 PLWH, n=14 PLw/oH) confirmed an exhausted $CD8^+$ T cell compartment, marked by enrichment of $PD1^{int}LAG3^-$ and $PD1^{int}LAG3^+$ subpopulations, along with a significant accumulation of immunosuppressive myeloid-derived suppressor cells ($CD11b^+$ $HLA\text{-}DR^-$ $CD33^+$) in PLWH.

These distinct immune profiles suggest chronic HIV infection fosters a permissive tumor microenvironment that might undermine effective immune responses and contribute to poor clinical outcomes for PLWH with melanoma. Targeting the actionable immune pathways identified in this study could inform tailored therapeutic strategies to mitigate these disparities.

Introduction

Advancements in antiretroviral therapies (ART) have transformed HIV infection from a fatal immunodeficiency into a manageable chronic condition, allowing people living with HIV (PLWH) to achieve a life expectancy nearly equal to that of the general population [1, 2]. However, despite the success of ART in suppressing viral replication and preventing acquired immunodeficiency syndrome (AIDS), HIV remains a lifelong infection due to its ability to integrate into host genomes and establish a state of latency, particularly within long-lived memory T cells and myeloid cells in sanctuary sites [3-6]. While ART prevents the spread of the infection, it does not eliminate pre-existing reservoirs that harbor integrated and latent viruses, leaving PLWH with persistent immune dysregulation and, therefore, increased susceptibility to age-related diseases [7]. Among these, non-AIDS-defining cancers (NADCs) have emerged as a major cause of mortality, including cutaneous melanoma [7]. Several reports on melanoma in PLWH point to disproportionately worse clinical outcomes compared to melanoma patients without HIV, despite adjustment for key factors such as disease

stage at presentation [8-11]. The mechanisms underlying this disparity remain poorly understood. In particular, it is largely unknown how chronic HIV infection alters anti-tumor immune responses, which are particularly critical for melanoma, given the central role of the immune system in the progression and response to treatment in this type of malignancy.

To address this major knowledge gap, we first analyzed publicly available clinical datasets to compare demographics and outcomes between PLWH and HIV-negative individuals (PLw/oH), revealing significant disparities in demographics, metastasis risk, and survival after a melanoma diagnosis. We then performed the first immune-focused spatial transcriptomic analysis of melanoma tumors according to patient HIV status, uncovering striking differences in T cell and myeloid populations in PLWH. These findings were further validated and expanded using multiplex immunofluorescence to characterize immune cell phenotypes and subpopulations. Together, our data reveal a profoundly altered immune landscape in melanoma among PLWH, marked by T cell exhaustion and myeloid-mediated suppression, which underscores the need for tailored therapeutic strategies in this population with suboptimal clinical outcomes.

Results

PLWH with melanoma display increased overall mortality rates and brain metastasis risk.

To evaluate population differences between PLWH and PLw/oH diagnosed with melanoma, we interrogated the TriNetX US Collaborative Network dataset. Our study included two cohorts: 922 PLWH with melanoma and 334,972 melanoma patients without HIV. Baseline demographic analysis revealed that PLWH were diagnosed with melanoma at a younger age (58.4 ± 12.3 years in PLWH vs. 62.8 ± 15.6 years in PLw/oH) and were more likely to be male (80% vs. 52%, **Table 1**). Racial and ethnic distribution also differed between the cohorts. PLWH with melanoma exhibited a higher representation of Hispanic or Latino individuals (4% vs. 1%) and Black or African American individuals (7% vs. 1%) compared to their non-HIV counterparts (**Table 1**).

Regarding survival outcomes, both five-year (84.13% vs 86.50% survival rate, PLWH vs. PLw/oH, p=0.0266) and ten-year (70.07% vs 77.22% survival rate, PLWH vs. PLw/oH, p=0.0007) survival rates were considerably lower in PLWH (**Fig 1A-B**, **Table S1-2**), suggesting a worse long-term prognosis, consistent with previous reports [8]. The two cohorts had a similar median follow-up time of approximately 3.2 (PLw/oH) and 4.2 years (PLWH, **Table S3**), and our analysis focused on patients diagnosed during the HAART era (98.4% of patients had HAART treatment records). Given the impact of metastasis on cancer mortality, we assessed the risk of melanoma spreading to its most frequent metastatic sites. No significant differences were detected between the two groups of patients in terms of metastasis at presentation/early metastasis (0 days to 6 months after diagnosis, **Table 2**). Interestingly, while there were no significant differences in lung, liver, or lymph node metastases, PLWH had a significantly higher risk of late brain metastases (>6 months after diagnosis, p<0.0001, risk ratio = 1.98, **Table 2**), and an overall increased risk of metastatic disease in the long term (p<0.0001, risk ratio = 1.484, **Table 2**).

Next, we focused on FDA-approved immune checkpoint inhibitors (ICIs) to evaluate differences in treatment patterns and outcomes between the two groups. ICIs serve as the first-line treatment approach

for patients with advanced melanoma, and analyzing their use provides insights into how patients with late-stage disease fare in the clinical setting. Among our cohorts, approximately 8% of PLWH (n=75) and 6% of PLw/oH (n=18,361) had a record of receiving immune checkpoint therapies. The demographic features of these two sub-groups reflected the differences we detected between the parent cohorts (**Table 3**). Although we were not statistically powered enough to draw conclusions for specific treatment regimens, we were able to make some comprehensive observations regarding ICI outcomes and timing. We found that, on average, PLWH experienced longer delays before initiating treatment compared to PLw/oH (p=0.0099, **Table 3**). This is consistent with existing knowledge that PLWH face barriers to timely treatment, possibly due to differences in healthcare access, treatment prioritization, or delays in clinical decision-making. Once ICI was initiated, we did not detect differences in treatment duration (**Table 3**). We then performed five- and ten-year survival analyses of the two cohorts. At both time points, PLWH demonstrated significantly lower probabilities of survival compared to the non-HIV melanoma patients (5-year, 54.85% vs 65.84% survival rate, PLWH vs. PLw/oH, p=0.0276; 10-year, 32.81% vs 47.92% survival rate, PLWH vs. PLw/oH, p=0.0179, **Fig. 1C-D**, and **Table S4-5**).

PLWH display an immune suppressive and exhausted melanoma tumor microenvironment

Our data indicate that PLWH who develop melanoma experience an overall elevated mortality rate. While demographic differences, higher rates of coexisting conditions, and psychosocial barriers are contributors to mortality, the decreased survival rate even after ICI indicates there may also be underlying biological or immunological components. To explore this, we collected tumor samples from 11 PLWH with melanoma and matched them with samples from 11 patients without HIV (PLw/oH) with melanoma (**Table S6**).

For each sample, we processed three to five regions of interest (ROIs) for spatial immune transcriptomics (72 immune-related genes). A pathologist selected the ROIs based on morphology and the expression of melanocytic markers, labeling subregions as either "tumor-cell rich" (TUMOR) or "tumor-microenvironment rich" (TME). To identify differences in gene expression between PLWH and PLw/oH, we performed differential expression analysis (DEGs) using the DEseq2 algorithm, comparing the TME and TUMOR regions. The analysis revealed significant gene expression differences between the groups, suggesting distinct immunological characteristics associated with HIV status (**Fig 2**).

When comparing the TME and TUMOR areas of PLWH with PLw/oH, we observed increased expression of several immune checkpoint genes, including *PD1*, *LAG3*, *CTLA4*, *TIGIT*, *CD276* and *ICOSLG*. Notably, *LAG3* emerged as the top-scoring immune checkpoint in the TUMOR, while *PD1* was the highest in the TME (**Fig 2A-B**). This suggests that there are distinct spatial distributions of varying T cell populations within these tumors. Both the TUMOR and TME exhibited additional characteristics of an immune-suppressive or evasive microenvironment. In the TUMOR compartment, we observed elevated expression of *IDO1*, a key protein that inhibits T-cell function (**Fig 2A**). Meanwhile, the TME showed reduced expression of *HLA-DRB* and *B2M,* which are MHC class II and I molecules essential for antigen presentation (**Fig 2B**). Several key genes involved in immune responses were also downregulated,

including *IFNGR1*, *CD74*, *LY6E*, and *STAT2*. Beyond immune regulation, we identified an interesting pattern of differential gene expression pertaining to fibrosis and extracellular matrix (ECM) remodeling in the TME. PLWH demonstrated a decline in the expression of *CD44*, *ITGAV*, *and PECAM1* and increased *ITGB8*, suggesting alterations in tumor-stroma interactions that may contribute to disease progression (**Fig 2B**).

Interestingly, a small cadre of genes associated with enhanced inflammation was identified in the TME of PLWH, including an increase in *IL-15*, *TBX21*, and *CCL5* (**Fig 2B**). In the TUMOR, there was an increase in *BATF3*, which is mostly expressed on $CD8^+$ cells, (i.e., dendritic cells and T cells) (**Fig 2A**).

To summarize our findings and prioritize downstream validation, we ran a modified version of the MCPcounter algorithm, utilizing tailored gene sets, including population marker genes and immune signaling genes (**Table S7-8**). The only two upregulated gene sets in PLWH, both in TME and TUMOR areas, were immune checkpoints and myeloid suppressive signaling (**Fig 2C**). In terms of immune populations, overall, it appeared that the TUMOR areas from PLWH were generally enriched in immune cells both from myeloid and lymphoid origin, and displayed enhanced expression of several immune signaling pathways (**Fig 2C** and **Fig S1**). The TME areas were, in general, more similar between PLWH and PLw/oH (**Fig S1**).

PLWH display distinct subsets of $CD8^+$ T cells within the melanoma tumor environment

To validate and further expand upon the spatial transcriptomics findings, we investigated T cell populations using multiplexed immunofluorescence staining (mIF). The cohort included melanoma tumor samples from 15 HIV^+ and 14 HIV^- patient samples, with 11 samples in each group overlapping with those profiled by spatial transcriptomics. We examined T cell populations within both the tumor bulk and peripheral edges using an mIF panel targeting T cell populations (CD8, CD4, Foxp3), along with the two top-scoring immune checkpoint inhibitors identified in our transcriptional analysis (LAG3 and PD1) (**Fig 3A**). Melanocytic markers were not included in this panel; thus, the results reflect the tumor specimens as a whole instead of specific delineation of sub-regions.

Analysis of the T cell compartment revealed no significant differences in the overall frequency of $CD8^+$ or $CD4^+$ T cells between melanoma tumors in PLWH and uninfected patients (**Fig 3B-C**). Similarly, regulatory T cells (T_{REG}, $CD4^+FOXP3^+$) abundance did not differ significantly between groups (**Fig S2A**). Notably, PLWH exhibited altered T cell proportions, with a significantly reduced $CD4^+$:$CD8^+$ ratio and a lower $Foxp3^+$:$CD8^+$ ratio, suggesting a shift in the relative balance of T cell subsets (**Fig 3D-E**).

We next interrogated the co-expression of immune checkpoint receptors PD1 and LAG3 on $CD4^+$ and $CD8^+$ T cells. PD1 expression was stratified into three tiers ($PD1^-$, $PD1^{int}$, and $PD1^{high}$), and LAG3 into two ($LAG3^-$ and $LAG3^+$), based on previous reports highlighting functional differences in cytotoxicity and exhaustion in these subpopulations [12-15]. No significant differences were observed in $CD4^+$ T cell subsets between PLWH and uninfected patients (**Fig S2B-E**).

Interestingly, we identified distinct subpopulations of $CD8^+$ T cells in PLWH compared PLw/oH. Specifically, melanoma tumors from PLWH showed significant enrichment of the $CD8^+PD1^{int}$ $LAG3^-$ and the

$CD8^+PD1^{int}$ $LAG3^+$ populations (**Fig 3F-G**). Notably, we did not detect any differences in the abundance of $PD1^{high}$ cells, whether they were $LAG3^+$ or $LAG3^-$ (**Fig 3H-J**).

Given the important role of the myeloid compartment in modulating T cell function, we next turned our focus to tumor-associated myeloid populations.

PLWH exhibit an enriched population of immunosuppressive myeloid cells in melanoma tumors

The selection of myeloid markers for downstream analysis was guided by multiple converging lines of evidence. Pathway analysis highlighted myeloid suppressive signaling as a top candidate (**Fig. 2C**) and a significant downregulation of key components of antigen presentation, such as *HLA-DRB*, within the tumor regions (**Fig. 2**). In parallel, previous studies have reported that PLWH have elevated levels of myeloid-derived suppressor cells (MDSCs) at baseline, a population of highly immunosuppressive, immature myeloid cells [16, 17]. Based on these findings, we selected CD11b to broadly define the myeloid lineage and included HLA-DR, CD33, and CD66b to resolve functional subpopulations, including potential MDSCs. Using multiplexed immunofluorescence (mIF) on the tumor samples previously analyzed for T cell populations, we identified a significant increase in $CD11b^+$ $HLA\text{-}DR^-$ myeloid cells in PLWH (**Fig. 4B**), consistent with an immature or non-antigen-presenting phenotype. Most of these cells also expressed CD33, supporting their classification as monocytic-like MDSCs (M-MDSCs) (**Fig. 4C**). In contrast, no differences were observed in $CD11b^+$ $HLA\text{-}DR^-$ $CD66b^+$ cells, or polymorphonuclear-like MDSCs (PMN-MDSC) between PLWH and PLw/oH (**Fig. 4D**) [18].

Discussion

The present study demonstrates that PLWH who develop melanoma experience distinct clinical outcomes and tumor microenvironments compared to those without HIV. Notably, PLWH exhibited increased overall mortality, including in the subpopulation of patients who underwent ICI. Immune-focused spatial transcriptomics analysis revealed substantial immune exhaustion in the T cell compartment and the upregulation of several immune suppressive markers. Multiplex immunofluorescence further identified an enrichment of unique $CD8^+$ T cell subsets, indicating a skewed T cell response profile, alongside an increased presence of MDSCs, which are known to inhibit T cell function and promote immune suppression.

Our results highlight the unique immunological features in melanoma tumors of PLWH, emphasizing the need for updated targeted interventions. Despite the growing use of ICI in melanoma and several reports demonstrating safety in PLWH [19], this patient population was largely excluded from oncology clinical trials, resulting in a significant gap in reliable data regarding the efficacy of ICI use within this population [20-22]. This exclusion fosters a cycle of provider hesitancy and continued research omission, ultimately limiting access to optimal cancer care and contributing, in part, to increased melanoma mortality [20]. Consistent with these challenges, our study demonstrates that PLWH experience significantly longer delays in treatment initiation compared to individuals without HIV. This exacerbates disease progression

and can contribute to the increased melanoma mortality rate in PLWH that we report here. This delay likely stems from both the clinical uncertainty due to the lack of clinical trial data and psychosocial barriers, including healthcare access disparities and medical mistrust linked to historical HIV-related stigma, as we have previously reviewed [23]. Addressing these barriers is critical to improving melanoma outcomes for PLWH.

Additionally, our findings indicate a significantly higher risk of metastasis in the long-term in PLWH, especially brain metastasis, suggesting a potential immune surveillance vulnerability that facilitates melanoma dissemination and/or outgrowth to the brain. HIV infiltrates the brain early in the infection, contributing to chronic neuroinflammation and the development of HIV-associated neurocognitive disorder (HAND) [24]. This disruption of the blood-brain-barrier may create a permissive environment for melanoma cells to colonize there [25]. This increased risk highlights the importance of heightened cancer surveillance and early treatment strategies for this population, as literature shows that the occurrence of brain metastasis significantly lowers the probability of survival and response to therapy [26-28].

The observation that PLWH who underwent ICI also show decreased survival rates might indicate that ICI does not induce as durable responses in this population as in PLw/oH, especially because time on treatment was similar between the two populations. Importantly, none of the PLWH patients in the ICI cohort received targeted therapy before ICI, which is a known factor affecting treatment response [29].

In addition to detailing the clinical characteristics of melanoma in PLWH, our study provides critical insights into how chronic HIV infection fundamentally alters the tumor immune landscape, potentially driving worsened outcomes for this population of patients. The complex landscape of immune dysfunction within the melanoma TME of PLWH is underscored by our identification of two enriched $CD8^+$ T cell subsets: $CD8^+$ $PD1^{INT}$ $LAG3^+$ and $CD8^+$ $PD1^{INT}$ $LAG3^-$.

PD1 and LAG3 are inhibitory receptors upregulated on $CD8^+$ T cells during chronic viral infections and within tumors. Although both initially serve as markers of T cell activation, sustained expression, especially in combination, drives T cell exhaustion. The similar frequencies of $CD8^+$ $PD1^{HIGH}$ T cells observed in both PLWH and PLw/oH likely reflect common chronic stimulation by tumor antigens or PD-L1 expression [30-32]. In contrast, the increased abundance of $CD8^+$ $PD1^{INT}$ $LAG3^{+/-}$ T cells in PLWH points to a population of recently activated cells. The presence of LAG3 co-expression in one of the subsets suggests that these cells are transitioning from an activated state toward exhaustion. Specifically, the $CD8^+$ $PD1^{INT}$ $LAG3^-$ population may represent an activated but pre-exhausted phenotype, with their ultimate functional fate influenced by local tumor-derived cues. Supporting this interpretation, spatial transcriptomic analysis revealed elevated *LAG3* transcription localized near tumor cells, consistent with a spatially driven gradient of exhaustion. Notably, co-expression of PD1 and LAG3 on $CD8^+$ T cells has been linked to impaired anti-tumor immunity. While dual blockade of PD1 and LAG3 has shown promise in improving progression-free survival in metastatic melanoma [33-36], clinical data on ICI efficacy in PLWH remain scarce, particularly for anti-LAG3 therapies. The dynamic interplay between LAG3 and PD1 in these subsets underscores the need for further research to determine their precise roles in tumor progression

and immune escape. Understanding these interactions could inform targeted therapies to restore effective anti-tumor immunity in PLWH.

Despite HIV's well-documented impact on the $CD4^+$ T cell compartment [37, 38], we observed no significant differences in total $CD4^+$ T cell counts or their subsets between cohorts, suggesting that immune dysregulation in the TME of PLWH is primarily driven by $CD8^+$ T cells. This is further supported by a decreased CD4:CD8 ratio in PLWH.

Distinct $CD8^+$ T cell subsets, combined with stable overall T cell numbers, suggest an immune landscape shaped by chronic antigen stimulation and exhaustion. However, T cell exhaustion is not the sole barrier to anti-tumor immunity in PLWH. Chronic HIV infection disrupts both adaptive T cell and innate myeloid cell compartments. We observed a significant downregulation of antigen presentation genes and a shift from classical to cross-presentation mechanisms, indicative of an immune-evasive or immunosuppressive myeloid phenotype [39-41]. Multiplex immunofluorescence analysis of the myeloid compartment revealed a significantly higher concentration of $CD11b^+HLA\text{-}DR^-CD33^+$ cells in melanoma tumors of PLWH. These cells, defined as myeloid-derived suppressor cells (MDSCs), are a rare and potent immunosuppressive subset of immature myeloid cells. In healthy individuals, MDSCs typically emerge later in cancer progression, where they are well-known contributors to immune evasion and immunotherapeutic resistance [42, 43]. However, PLWH exhibit elevated baseline levels of circulating MDSCs, regardless of ART status, likely due to chronic low-level inflammation [16, 18]. The recruitment of MDSCs to the melanoma tumor site, fueled by their elevated baseline levels in the peripheral circulation of PLWH, may facilitate a more rapid and aggressive trajectory of melanoma progression in this population [16-18, 44-46]. Our data support this hypothesis, as we observed an upregulation in the expression of *CCL5* in both TUMOR and TME areas. CCL5 is primarily recognized for its proinflammatory properties and its role in HIV pathogenesis, as a binding partner for CCR5, a co-receptor essential for HIV entry into host cells [47-50]. However, several studies have linked CCL5 to the recruitment of MDSCs, including in melanoma [51-53]. Elevated MDSC levels prior to initiating immunotherapy in melanoma patients have been associated with poorer treatment response and reduced overall survival, and $CD11b^+HLA\text{-}DR^-CD33^+$ cells have emerged as a predictive biomarker for advanced-stage melanoma prognosis [54]. Collectively, our findings suggest that MDSCs play a central role in shaping the tumor landscape of PLWH and highlight the need for further investigation into their impact on $CD8^+$ T cell responses, melanoma progression, and treatment outcomes.

Our investigation demonstrates that, despite effective ART, HIV infection fundamentally alters melanoma progression, as evidenced by heightened exhausted $CD8^+$ T cell subsets and an immunosuppressive myeloid cell presence within the tumors. These immune disruptions, combined with delayed healthcare responses and an increased risk for metastasis, likely contribute to the elevated mortality rate observed in PLWH. Collectively, these findings underscore the urgent need for inclusive clinical trials and targeted therapeutic strategies to address the unique challenges faced by PLWH and improve cancer outcomes for this population.

Methods

Clinical electronic record patient dataset

The data used in this study was collected 04/02/2025 from the TriNetX US Collaborative Network, which provided access to electronic medical records (diagnoses, procedures, medications) from approximately 109,330,986 patients from 67 healthcare organizations. Patient demographics include date of birth, age, sex, marital status, race, and ethnicity. Demographics are coded to HL7 version 3 administrative standards. For the survival studies, the date a patient was reported as “Deceased” in the dataset was used; the cause of death was not available in the dataset. The “Deceased” term in the TriNetX data model pools together several different sources of mortality data: documented mortality by HCOs using ICD-10 code R99 (ill-defined and unknown cause of mortality); if mortality is reported from HCOs via death dates of patients, this is also captured and mapped to the “Deceased” term; for the subset of patients on the TriNetX networks that have additional mortality data linked to their electronic health records (closed claims, social security master death file, private obituaries, etc.), these additional sources are also mapped to the “Deceased” term. Diagnoses and medication data in the TriNetX database are obtained from electronic health records of participating healthcare organizations. Diagnoses are recorded using the ICD-10 standardized coding system, while medication information is captured through prescription and dispensing records. These data may originate from clinical documentation, problem lists, billing records, or insurance claims and are harmonized across sites to ensure consistency.

Two cohorts of patients were retrieved with the following criteria: PLWH cohort was built selecting patients that had Malignant melanoma of skin (ICD code C43) and Human immunodeficiency virus [HIV] disease (ICD code B20, 922 patients were retrieved); PLw/oH cohort was built selecting patients that had C43 but not code B20 (334,972 patients were retrieved). Only patients with a cancer diagnosis between 2005 and 2025 were included. Only patients with a cancer diagnosis after HIV were included in the PLWH cohort.

The following ICD codes were used for metastatic disease: C78.7 (liver and bile duct), C79.3 (brain and meninges), C77 (lymph nodes), and C78.0 (lung). Two different analyses were performed for patients with an early occurrence of metastatic disease (from day 0 to 6 months after diagnosis) and patients with a later occurrence of metastasis (6 months from melanoma diagnosis onwards). For the “All sites” category, patients who had any of the metastatic codes C77, C78.0, C79.3, and C78.7 were included. In the dataset, medications are represented at the level of ingredients, coded to RxNorm, and organized by VA or ATC classification. For the analysis of immunotherapy characteristics and outcomes, the two cohorts were filtered to include only patients who had received any of the following FDA-approved immune checkpoint inhibitors: 1094833 (ipilimumab), 1597876 (nivolumab),1547545 (pembrolizumab), 1792776 (atezolizumab), 1919503 (durvalumab) or 2596773 (relatlimab).

This retrospective study is exempt from informed consent. The data reviewed is a secondary analysis of existing data, does not involve intervention or interaction with human subjects, and is de-identified per the de-identification standard defined in Section §164.514(a) of the HIPAA Privacy Rule. The process by which the data is de-identified is attested to through formal determination by a qualified expert

as defined in Section §164.514(b)(1) of the HIPAA Privacy Rule. This formal determination by a qualified expert was refreshed in December 2020.

Patient tumor samples

De-identified melanoma patient samples were acquired from the AIDS and Cancer Specimen Resource, the Sidney Kimmel Comprehensive Cancer Center, and NYU Grossman School of Medicine. Melanoma samples from people living with HIV were retrieved first, and HIV-uninfected controls were then selected to match age, sex, race and ethnicity, and nature of specimens.

Spatial Immune Transcriptomics

Five-micron sections were prepared after thoroughly cleaning the microtome and recovering sections in RNAse free water. Slide preparation was performed following the NanoString® standard of practice for nCounter RNA GeoMx experiments. Briefly, slides were baked for 2 hours at 60°C before being loaded onto a BOND Rx automated slide stainer (Leica Biosystems). Slides underwent baking, dewaxing, and heat-induced antigen retrieval with an EDTA based (pH9) solution (ER2 Leica, Cat. AR9640) for 20 minutes at 100 °C, followed by proteolytic-induced epitope retrieval with proteinase K (Ambion, Cat. AM2546) at a 1ug/ml concentration for 15 minutes at ambient temperature. After antigen retrieval, slides were moved to PBS until overnight probe incubation. Slides were incubated overnight with 200 µL of nCounter GeoMx Immune Pathways Hs RNA Probes (Cat. 121300201, Lot: 20211122) in a HybEZ™ oven at 37°C. Slides were covered with a Hybrislip (Grace biolabs, Cat. 714022) to ensure uniform reagent distribution. Next, the slides underwent two stringent washes in 50% (v/v) Formamide-4XSSC at 37°C, then two washes in 2XSSC at room temperature. Slides were then immunofluorescently labeled with RNA-compatible melanoma morphology markers (GeoMx Melanoma Morph Kit Hs RNA, NanoString® cat.121300311, lots: S100B/PMEL-AF 532 230413-01, 210807-02; Nuclear Syto13 20230621, 210807-02). All slides were stained and hybridized at the same time. However, loading onto the GeoMx instrument and collection was done in batches of 4 slides. On the instrument, automated wide field fluorescence imaging was performed with epi-illumination from visible LED at 20X magnification (0.4 µm/px). The 20x images were stitched together to yield a high-resolution image of the tissue area of interest. Regions of interest (ROI) were then selected based on the fluorescence information and sequentially processed by the instrument automation. Three to five ROIs were selected for each sample. A pathologist selected the ROIs based on morphology and the expression of melanocytic markers, labeling subregions as either "tumor-cell rich" (TUMOR) or "tumor-microenvironment rich" (TME). The area of tissue within the ROI was precisely illuminated with UV light (~1 μm^2 resolution) to release the barcodes from the hybridized probes. Following each UV illumination cycle, the eluent was collected from the local region via microcapillary aspiration and transferred to an individual well of a 96-well microtiter plate. Once all ROIs were acquired, the multi-well plates were covered and stored at -20°C until nCounter processing at NYUGSM Genome Technology Center. For each plate containing the eluted tags from each ROI the following workflow was performed. Plates were covered with a semi-permeable seal and heated to 65°C for 1-2 hours to lyophilize the sample.

Once the entire plate was dry, the samples were rehydrated in 7ul DEPC water. The ICP pool was diluted with nuclease-free water to create a working stock and added to a hybridization buffer to create the ICP-hyb mix. This mix was added to each tube of GeoMx Hyb Code Pack_RNA (tubes A-H) (Cat. 121300402). In new plates, the mix was plated in a row across a plate as follows- tube A (8ul) is added to wells A1-A12 across the plate, tube B is added to wells B1 to B12 etc. rehydrated RNA (7ul) was added to the new plate containing the probe-hyb mix in the same well resulting in 15ul total (RNA sample in well A1 was added to the plate containing probe set well A1 etc.). The plate was sealed and incubated overnight at 65°C for up to 24h. The following day, the plate was cooled on ice and pooled in entire columns into a new well of a strip tube (A1-H1 combined, A2-H2 combined, etc). The combined strip tube containing all 96 wells with hybridized pools was run in the nCounter MAX/Flex system to generate RCC files. The RCC files were transferred back to the GeoMx control center to assess read counts for each plate. The abbreviated annotation can be found in the GeoMx-nCounter RNA/DSP readout quick start guide version MAN-10104-04. Read counts were normalized to the geometric mean of 5 housekeeping genes (OAZ1, POLR2A, RAB7A, SDHA, UBB). Normalized read counts are reported in **Table S7**. Differential expression analysis (DEGs) was conducted on the normalized read counts using the DEseq2 algorithm [55] in R v4.4.2 to compare the TME and TUMOR across HIV-positive and HIV-negative patients.

Immune pathways and population analysis

The MCP-counter algorithm was used to calculate the enrichment scores of tailored gene sets. [56]. We analyzed the dataset in two different ways: a marker-genes based analysis to detect differences in an immune signaling-genes based analysis (53 genes, **Table S8**) and immune population abundances (19 genes, **Table S9**). A multiple Welch t-test was then performed on the population or pathway scores in HIV+ vs. HIV- samples. Data were represented in a bubble plot with the adjusted p-value (q-value) and Log2 fold change (HIV+ vs. HIV-) for the TUMOR and TME areas (R v4.4.2; ggplot2 package).

Multiplex Immunofluorescence (mIF)

Multiplex immunofluorescence staining was performed on 5 µm paraffin sections with Akoya Biosciences® Opal™ reagents on a Leica BondRx autostainer, according to the manufacturer's instructions. T cell and myeloid infiltrates were assessed using two antibody panels: Panel 1 (CD8, CD4, FoxP3, Lag3, PD1, **Table S10**) and Panel 2 (CD11b, CD33, HLA-DR, CD66b, **Table S11**). In brief, sections were first treated with hydrogen peroxide to inhibit endogenous peroxidases, followed by an antigen retrieval step with ER2 (Leica AR9640) at 100°C. Slides were incubated with the first primary and secondary antibody pair and then underwent HRP-mediated tyramide signal amplification with a specific Opal® fluorophore. The primary and secondary antibodies were subsequently removed with a heat retrieval step, leaving the Opal fluorophore covalently linked in correspondence to the antigen location. This sequence was repeated with subsequent primary and secondary antibody pairs and a different Opal fluorophore at each step. Sections were counterstained with spectral DAPI (Akoya Biosciences, FP1490) and mounted with ProLong Gold Antifade (ThermoFisher Scientific, P36935). Semi-automated image

acquisition was performed on either a Leica AT2 whole slide bright field scanner at 40X magnification or on an Akoya Vectra Polaris (PhenoImagerHT) multispectral imaging system at 20X magnification using PhenoImagerHT 2.0 software in conjunction with Phenochart 2.0 and InForm 3.0 to generate unmixed whole slide qptiff scans. Digitized multiplex IF staining qptiff scans were analyzed using the open-source software QuPath [57]. Each analysis included four regions of interest (ROIs). Two were located at the center of the tumor bulk, and two at the tumor periphery. To ensure analytical rigor, two independent operators conducted the analyses. While both operators adhered to the same fixed-threshold detection methods, they independently selected the ROIs. ROIs on each section were averaged, and the averages of the two operators were considered as a replicate of the same data point. Total cells in ROI were detected with the QuPath automated cell detection algorithm based on DAPI color threshold and cell size/shape. For T cell analysis, $CD8^+$ and $CD4^+$ cells were quantified as a proportion of the total detected cells. The amount of $PD1^+$, $LAG3^+$, and/or $FOXP3^+$ cells in the CD8 and CD4 compartments was expressed as a percentage of the total number of cells in the analyzed areas. For myeloid cell analysis, $CD11b^+$ cells were identified, and their co-expression with HLA-DR, CD33, or CD66b was assessed and expressed as a percentage over the total number of cells in the area.

Statistical analysis

Data was checked for normality (Kolmogorov-Smirnov, Shapiro-Wilk test) prior to being assigned to parametric or non-parametric analyses. All the datasets analyzed in this work displayed normal distribution. To compare significant differences between two groups, we used a two-tailed t-test (parametric; Welch correction was applied if variances were different between groups). A $p<0.05$ was considered significant. For the immune pathways and population analysis, a multiple Welch t-test was performed with an FDR of 0.01. An adjusted p-value (q-value)<0.01 was considered significant. For survival studies, a Log-rank (Mantel-Cox) test was used to detect differences in survival between two populations. A $p<0.05$ was considered significant. For risk Ratio assessment, risk ratios with 95% confidence intervals are calculated to compare outcomes between cohorts. Risk was defined as the percentage of patients in the cohort who have the outcome in the time window (Risk = Patients with Outcome/Patients in Cohort). Risk Ratio was defined as the ratio of risk between cohorts (Risk Ratio = Risk for Cohort 1 / Risk for Cohort 2). TriNetX Live was utilized to perform all the population analyses. GraphPad Prism v.10.4.1 was utilized to perform all the other statistical tests.

References.

1. Deeks, S.G., S.R. Lewin, and D.V. Havlir, *The end of AIDS: HIV infection as a chronic disease.* Lancet, 2013. **382**(9903): p. 1525-33.
2. Escota, G.V., et al., *Understanding mechanisms to promote successful aging in persons living with HIV.* Int J Infect Dis, 2018. **66**: p. 56-64.
3. Cantero-Perez, J., et al., *Resident memory T cells are a cellular reservoir for HIV in the cervical mucosa.* Nat Commun, 2019. **10**(1): p. 4739.
4. Murray, A.J., et al., *The Latent Reservoir for HIV-1: How Immunologic Memory and Clonal Expansion Contribute to HIV-1 Persistence.* J Immunol, 2016. **197**(2): p. 407-17.
5. Cohn, L.B., et al., *HIV-1 integration landscape during latent and active infection.* Cell, 2015. **160**(3): p. 420-32.
6. Wahl, A. and L. Al-Harthi, *HIV infection of non-classical cells in the brain.* Retrovirology, 2023. **20**(1): p. 1.
7. Eyawo, O., et al., *Changes in mortality rates and causes of death in a population-based cohort of persons living with and without HIV from 1996 to 2012.* BMC Infect Dis, 2017. **17**(1): p. 174.
8. Yuan, T., et al., *Incidence and mortality of non-AIDS-defining cancers among people living with HIV: A systematic review and meta-analysis.* EClinicalMedicine, 2022. **52**: p. 101613.
9. Lurain, K., R. Yarchoan, and R. Ramaswami, *The Changing Face of HIV-Associated Malignancies: Advances, Opportunities, and Future Directions.* Am Soc Clin Oncol Educ Book, 2019. **39**: p. 36-40.
10. Coghill, A.E., et al., *Advanced stage at diagnosis and elevated mortality among US patients with cancer infected with HIV in the National Cancer Data Base.* Cancer, 2019. **125**(16): p. 2868-2876.
11. Coghill, A.E., et al., *Elevated Cancer-Specific Mortality Among HIV-Infected Patients in the United States.* J Clin Oncol, 2015. **33**(21): p. 2376-83.
12. Yang, Z.Z., et al., *Expression of LAG-3 defines exhaustion of intratumoral PD-1(+) T cells and correlates with poor outcome in follicular lymphoma.* Oncotarget, 2017. **8**(37): p. 61425-61439.
13. Guegan, J.P., et al., *Analysis of PD1, LAG3, TIGIT, and TIM3 expression in human lung adenocarcinoma reveals a 25-gene signature predicting immunotherapy response.* Cell Rep Med, 2024. **5**(12): p. 101831.
14. Maruhashi, T., et al., *LAG-3: from molecular functions to clinical applications.* J Immunother Cancer, 2020. **8**(2).
15. Grosso, J.F., et al., *Functionally distinct LAG-3 and PD-1 subsets on activated and chronically stimulated CD8 T cells.* J Immunol, 2009. **182**(11): p. 6659-69.
16. Qin, A., et al., *Expansion of monocytic myeloid-derived suppressor cells dampens T cell function in HIV-1-seropositive individuals.* J Virol, 2013. **87**(3): p. 1477-90.
17. Singh, R., et al., *Residual immune activation in HIV-Infected individuals expands monocytic-myeloid derived suppressor cells.* Cell Immunol, 2021. **362**: p. 104304.
18. Bronte, V., et al., *Recommendations for myeloid-derived suppressor cell nomenclature and characterization standards.* Nat Commun, 2016. **7**: p. 12150.

19. El Zarif, T., et al., *Safety and Activity of Immune Checkpoint Inhibitors in People Living With HIV and Cancer: A Real-World Report From the Cancer Therapy Using Checkpoint Inhibitors in People Living With HIV-International (CATCH-IT) Consortium.* J Clin Oncol, 2023. **41**(21): p. 3712-3723.
20. Suneja, G., et al., *Cancer Treatment in Patients With HIV Infection and Non-AIDS-Defining Cancers: A Survey of US Oncologists.* J Oncol Pract, 2015. **11**(3): p. e380-7.
21. Vora, K.B., B. Ricciuti, and M.M. Awad, *Exclusion of patients living with HIV from cancer immune checkpoint inhibitor trials.* Sci Rep, 2021. **11**(1): p. 6637.
22. Knight, A., L. Karapetyan, and J.M. Kirkwood, *Immunotherapy in Melanoma: Recent Advances and Future Directions.* Cancers (Basel), 2023. **15**(4).
23. Barger, L.N., et al., *Melanoma in people living with HIV: Immune landscape dynamics and the role of immuno- and antiviral therapies.* Cancer Metastasis Rev, 2024. **44**(1): p. 9.
24. Saylor, D., et al., *HIV-associated neurocognitive disorder--pathogenesis and prospects for treatment.* Nat Rev Neurol, 2016. **12**(4): p. 234-48.
25. Thompson, L.J., et al., *HIV-Associated Neurocognitive Disorder: A Look into Cellular and Molecular Pathology.* Int J Mol Sci, 2024. **25**(9).
26. Kluger, H.M., et al., *Long-Term Survival of Patients With Melanoma With Active Brain Metastases Treated With Pembrolizumab on a Phase II Trial.* J Clin Oncol, 2019. **37**(1): p. 52-60.
27. Robert, C., et al., *Seven-Year Follow-Up of the Phase III KEYNOTE-006 Study: Pembrolizumab Versus Ipilimumab in Advanced Melanoma.* J Clin Oncol, 2023. **41**(24): p. 3998-4003.
28. Long, G.V., et al., *Combination nivolumab and ipilimumab or nivolumab alone in melanoma brain metastases: a multicentre randomised phase 2 study.* Lancet Oncol, 2018. **19**(5): p. 672-681.
29. Atkins, M.B., et al., *DREAMseq (Doublet, Randomized Evaluation in Advanced Melanoma Sequencing): A phase III trial—ECOG-ACRIN EA6134.* Journal of Clinical Oncology, 2021. **39**(36_suppl): p. 356154-356154.
30. Jiang, Y., Y. Li, and B. Zhu, *T-cell exhaustion in the tumor microenvironment.* Cell Death Dis, 2015. **6**(6): p. e1792.
31. Kaunitz, G.J., et al., *Melanoma subtypes demonstrate distinct PD-L1 expression profiles.* Lab Invest, 2017. **97**(9): p. 1063-1071.
32. Gangaev, A., et al., *Differential effects of PD-1 and CTLA-4 blockade on the melanoma-reactive CD8 T cell response.* Proc Natl Acad Sci U S A, 2021. **118**(43).
33. Andrews, L.P., et al., *LAG-3 and PD-1 synergize on CD8(+) T cells to drive T cell exhaustion and hinder autocrine IFN-gamma-dependent anti-tumor immunity.* Cell, 2024. **187**(16): p. 4355-4372 e22.
34. Huang, R.Y., et al., *LAG3 and PD1 co-inhibitory molecules collaborate to limit CD8+ T cell signaling and dampen antitumor immunity in a murine ovarian cancer model.* Oncotarget, 2015. **6**(29): p. 27359-77.
35. Tawbi, H.A., et al., *Relatlimab and Nivolumab versus Nivolumab in Untreated Advanced Melanoma.* N Engl J Med, 2022. **386**(1): p. 24-34.
36. Amaria, R.N., et al., *Neoadjuvant relatlimab and nivolumab in resectable melanoma.* Nature, 2022. **611**(7934): p. 155-160.
37. Okoye, A.A. and L.J. Picker, *CD4(+) T-cell depletion in HIV infection: mechanisms of immunological failure.* Immunol Rev, 2013. **254**(1): p. 54-64.
38. Kelley, C.F., et al., *Incomplete peripheral CD4+ cell count restoration in HIV-infected patients receiving long-term antiretroviral treatment.* Clin Infect Dis, 2009. **48**(6): p. 787-94.
39. Sugita, M. and M.B. Brenner, *An unstable beta 2-microglobulin: major histocompatibility complex class I heavy chain intermediate dissociates from calnexin and then is stabilized by binding peptide.* J Exp Med, 1994. **180**(6): p. 2163-71.
40. Sade-Feldman, M., et al., *Resistance to checkpoint blockade therapy through inactivation of antigen presentation.* Nat Commun, 2017. **8**(1): p. 1136.
41. Hildner, K., et al., *Batf3 deficiency reveals a critical role for CD8alpha+ dendritic cells in cytotoxic T cell immunity.* Science, 2008. **322**(5904): p. 1097-100.
42. Gabrilovich, D.I., *Myeloid-Derived Suppressor Cells.* Cancer Immunol Res, 2017. **5**(1): p. 3-8.
43. Wu, Y., et al., *Myeloid-derived suppressor cells: an emerging target for anticancer immunotherapy.* Mol Cancer, 2022. **21**(1): p. 184.
44. Wang, L., et al., *Expansion of myeloid-derived suppressor cells promotes differentiation of regulatory T cells in HIV-1+ individuals.* AIDS, 2016. **30**(10): p. 1521-1531.

45. Jordan, K.R., et al., *Myeloid-derived suppressor cells are associated with disease progression and decreased overall survival in advanced-stage melanoma patients.* Cancer Immunol Immunother, 2013. **62**(11): p. 1711-22.
46. Ostrand-Rosenberg, S. and C. Fenselau, *Myeloid-Derived Suppressor Cells: Immune-Suppressive Cells That Impair Antitumor Immunity and Are Sculpted by Their Environment.* J Immunol, 2018. **200**(2): p. 422-431.
47. Signoret, N., et al., *Endocytosis and recycling of the HIV coreceptor CCR5.* J Cell Biol, 2000. **151**(6): p. 1281-94.
48. Cocchi, F., et al., *Identification of RANTES, MIP-1 alpha, and MIP-1 beta as the major HIV-suppressive factors produced by CD8+ T cells.* Science, 1995. **270**(5243): p. 1811-5.
49. Liu, X., et al., *HIV-1 Nef induces CCL5 production in astrocytes through p38-MAPK and PI3K/Akt pathway and utilizes NF-kB, CEBP and AP-1 transcription factors.* Sci Rep, 2014. **4**: p. 4450.
50. Zeng, Z., et al., *CCL5/CCR5 axis in human diseases and related treatments.* Genes Dis, 2022. **9**(1): p. 12-27.
51. Zhang, Y., et al., *A novel role of hematopoietic CCL5 in promoting triple-negative mammary tumor progression by regulating generation of myeloid-derived suppressor cells.* Cell Res, 2013. **23**(3): p. 394-408.
52. Jackson, C., et al., *Distinct myeloid-derived suppressor cell populations in human glioblastoma.* Science, 2025. **387**(6731): p. eabm5214.
53. Schlecker, E., et al., *Tumor-infiltrating monocytic myeloid-derived suppressor cells mediate CCR5-dependent recruitment of regulatory T cells favoring tumor growth.* J Immunol, 2012. **189**(12): p. 5602-11.
54. Sade-Feldman, M., et al., *Clinical Significance of Circulating CD33+CD11b+HLA-DR- Myeloid Cells in Patients with Stage IV Melanoma Treated with Ipilimumab.* Clin Cancer Res, 2016. **22**(23): p. 5661-5672.
55. Love, M.I., W. Huber, and S. Anders, *Moderated estimation of fold change and dispersion for RNA-seq data with DESeq2.* Genome Biol, 2014. **15**(12): p. 550.
56. Becht, E., et al., *Estimating the population abundance of tissue-infiltrating immune and stromal cell populations using gene expression.* Genome Biology, 2016. **17**(1): p. 218.
57. Bankhead, P., et al., *QuPath: Open source software for digital pathology image analysis.* Sci Rep, 2017. **7**(1): p. 16878.

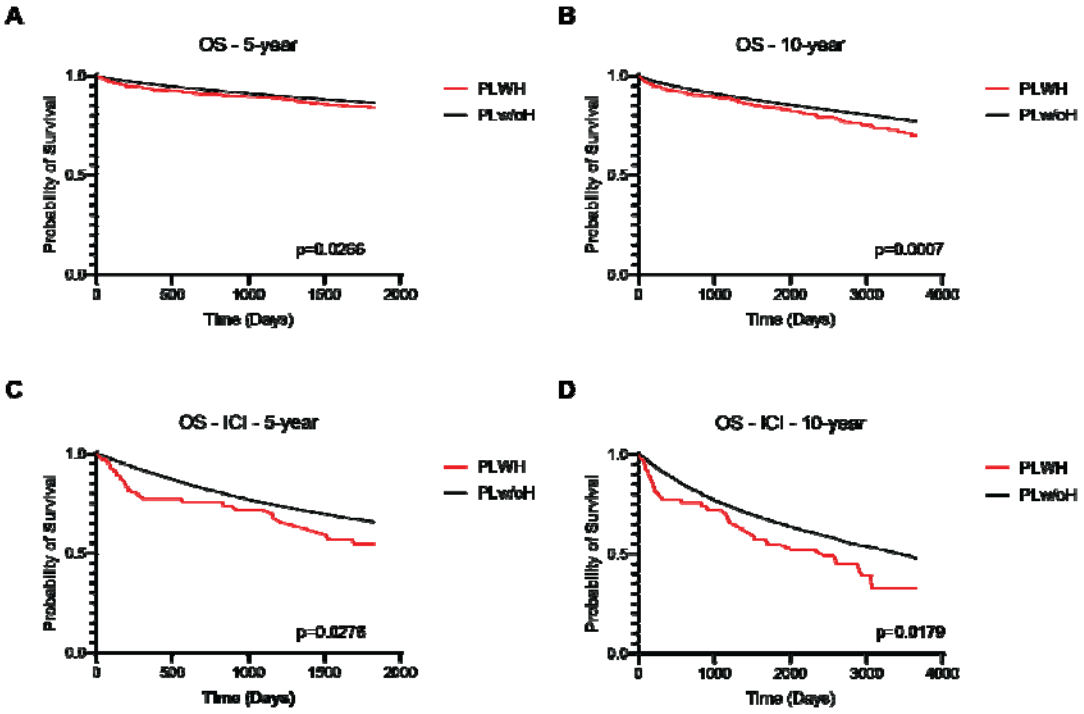

Figure 1. Overall survival rates and immune checkpoint therapy survival rates of PLWH and PLw/oH with melanoma. Kaplan-Meier graphs representing A) 5-year and B)10-year survival probability of PLWH and PLw/oH with melanoma. Kaplan-Meier graphs representing C) 5-year and D)10-year survival probability of PLWH and PLw/oH with melanoma who underwent immune checkpoint therapy. Reported p-values are from a Log-rank sum test between the two cohorts ($p<0.05$ is considered statistically significant).

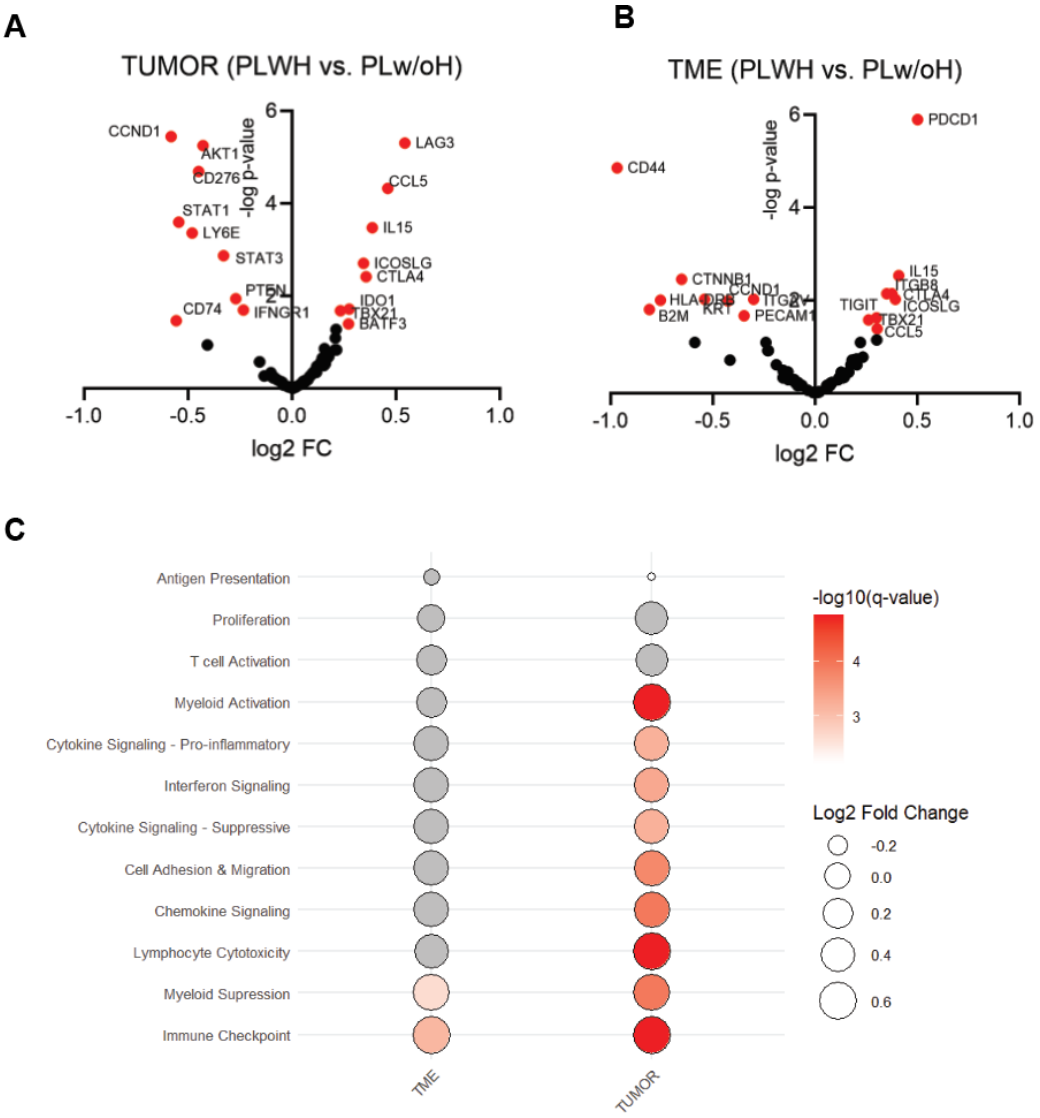

Figure 2. Spatial immune transcriptomic profiling of melanoma samples from PLWH and PLw/oH. Volcano plots for A) TME and B) TUMOR, comparing immune gene expression of PLWH vs PLw/oH melanoma samples (n=11); log2 fold change is on the x-axis, and -log10 of adjusted p-value is on the y-axis. Values were calculated by the DEseq2 algorithm (data points in red have an adjusted p-value <0.05). C) Bubble plot representation of immune signaling gene set analysis performed by running the MCPcounter algorithm on the gene expression matrix. Bubble plot size represents the log2 fold change of MCPcounter scores (PLWH vs. PLw/oH), and bubble color represents the adjusted p-value (q-value in a multiple Welch t-test with FDR of 0.01) for the TUMOR and TME areas (PLWH vs. PLw/oH). A q-value<0.01 was considered significant; comparisons with non-significant q-values are represented in grey.

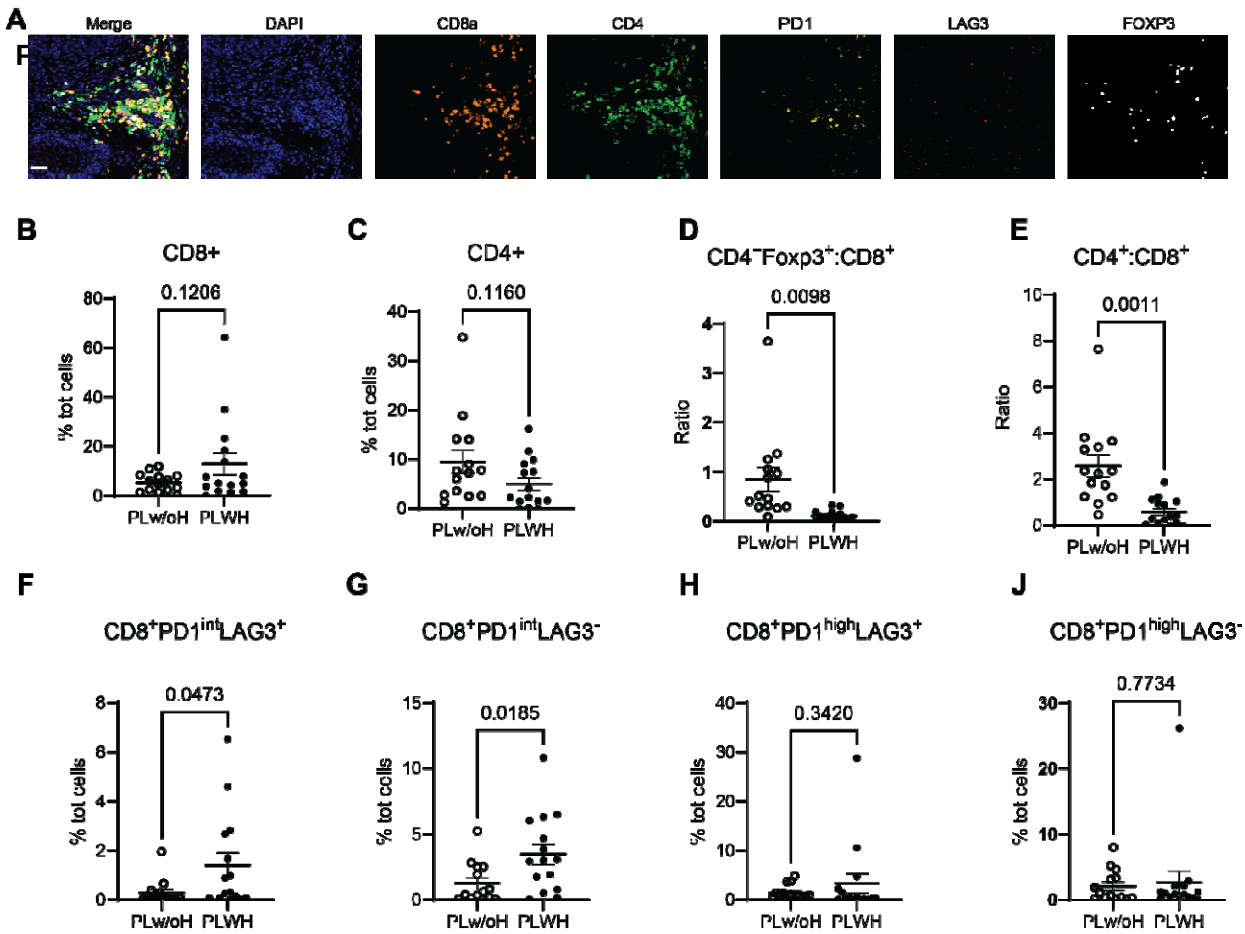

Figure 3. Multiplex IF assessment of T-cell populations' abundance and immune checkpoint expression in melanoma samples from PLWH and PLw/oH. A) Representative images of multiplex immunofluorescence (mIF) staining for the T cell panel in melanoma samples from PLWH and PLw/oH. The scale bar represents 50 µm. Quantification of mIF was performed on PLWH (n=15) and PLw/oH (n=14) tumor samples. Percentage of B) $CD8^+$ and C) $CD4^+$ T cells over the total number of cells. D) Ratio of $CD4^+Foxp3^+$ to $CD8^+$ T cells, and E) $CD4^+$ T cells to $CD8^+$ T cells. Percentage of $PD1^{int}$ $CD8^+$ T cells that are F) $LAG3^+$ and G)$LAG3^-$ over the total number of cells. Percentage of $PD1^{high}$ $CD8^+$ T-cells that are H) $LAG3^+$ and J) $LAG3^-$ over the total number of cells. The represented p-values are from a Welch's t-test; $p < 0.05$ is considered significant, and error bars represent SEM.

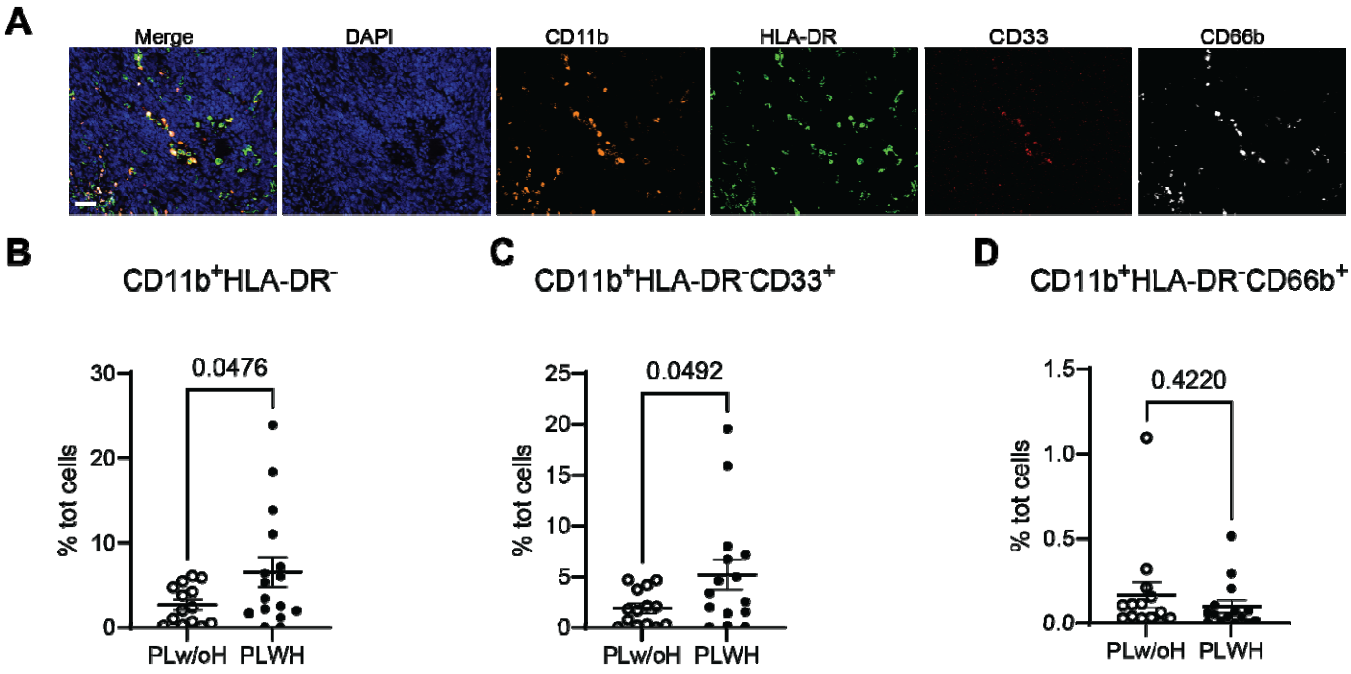

Figure 4. Multiplex IF assessment of myeloid populations' abundance in melanoma samples from PLWH and PLw/oH. A) Representative images of multiplex immunofluorescence (mIF) staining for the myeloid panel in melanoma samples from PLWH and PLw/oH. The scale bar represents 50 µm. Quantification of mIF was performed on PLWH (n=15) and PLw/oH (n=14) tumor samples. Percentage of B) $CD11b^{+}HLA\text{-}DR^{-}$, C) $CD11b^{+}HLA\text{-}DR^{-}$, $CD33^{+}$, D) $CD11b^{+}HLA\text{-}DR^{-}$, $CD66b^{+}$, over the total number of cells. The represented p-values are from a Welch's t-test; $p < 0.05$ is considered significant, and error bars represent SEM.